Acta Oceanol. Sin., 2017, Vol. 36, No. 8, P. 137–145
DOI: 10.1007/s13131-017-1032-0
http://www.hyxb.org.cn
E-mail: hyxbe@263.net

Paleoenvironmental implications of Holocene long-chain *n*-alkanes on the northern Bering Sea Slope

ZHANG Haifeng[1, 2], WANG Rujian[2]*, XIAO Wenshen[2]

[1] Laboratory of Marine Ecosystem and Biogeochemistry, State Oceanic Administration, Hangzhou 310012, China

[2] State Key Laboratory of Marine Geology, Tongji University, Shanghai 200092, China

Received 14 October 2016; accepted 28 April 2017

Abstract

The records of high-resolution terrestrial biological markers (biomarkers) from Core B2-9 from the northern Bering Sea Slope over the last 9.6 ka BP were presented in the study. Variations in input of terrestrial long-chain *n*-alkanes (referred to as *n*-alkanes) and vegetation structure in their source regions were investigated. The results show that the nC_{27} is the main carbon peak and has the greatest contribution rate of the total *n*-alkane content; this might be related to the abundance of woody plants and their spatial distribution in the source region. nC_{23} is another *n*-alkane having a relatively high content; this was mainly derived from submerged plants widespread along the coastal areas in the northern hemisphere. Total *n*-alkane content dropped quickly at ca. 7.8 ka BP, ca. 6.7 ka BP and ca. 5.4 ka BP, and was followed by four relatively stable stages mostly controlled by sea-level rise, climate change and vegetation distribution in the source region. Variation in carbon preference index (CPI) indicates that the *n*-alkanes primarily originated from higher land plants, and the average chain length (ACL) and nC_{31}/nC_{27} ratio reveal the relatively stable presence of woody/herbaceous plants during the Holocene, and dominate woody plants in most of the time. Simultaneous variation in total *n*-alkane content, nC_{27} content and its contribution, CPI, ACL and nC_{31}/nC_{27} ratio over several short periods suggest that the growth rate of the woody plant *n*-alkane contribution was lower than that of herbaceous plants and fossil *n*-alkanes under the particular climatic conditions of the source region.

Key words: Bering Sea, terrestrial input, long-chain *n*-alkanes, vegetation structure, Holocene

Citation: Zhang Haifeng, Wang Rujian, Xiao Wenshen. 2017. Paleoenvironmental implications of Holocene long-chain *n*-alkanes on the northern Bering Sea Slope. Acta Oceanologica Sinica, 36(8): 137–145, doi: 10.1007/s13131-017-1032-0

1 Introduction

The Bering Sea is the largest semi-closed marginal sea in the North Pacific. It is surrounded by the Aleutian Islands, East Siberia and Alaska, and is characterized by a wide continental shelf (<200 m) in its northeastern part (Fig. 1). With respect to the Pacific-Arctic-Atlantic gateway connection, the Bering Sea is significant in terms of water circulation, balances of heat and salt, and various chemical properties, which have great impact on global climate and mass balance (Takahashi, 1999). Hence, it has become the focus of keen interest for international paleoceanographers and paleoclimatologists (e.g., Takahashi, 1998; Wang et al., 2006; Gorbarenko et al., 2010).

Biomarkers have great potential in paleoenvironmental and paleoclimatic reconstructions (e.g., Hu et al., 2002; Lu et al., 2005; Zhao et al., 2006; Xing et al., 2008; Martínez-Garcia et al., 2009; Li, 2010; Rosell-Melé and Prahl, 2013; Hwang et al., 2014). *n*-Alkanes are branched saturated hydrocarbons with natural continuous carbon numbers and are common molecular biomarkers preserved in marine sediments. They are found widely in different kinds of plants and organisms and contain information relating to their biological origins (e.g., Meyers, 1997; Ficken et al., 2000; Mead et al., 2005); they can also indicate changes in vegetation structure and the paleoclimate in their source regions (e.g., Ohkouchi et al., 1997; Hu et al., 2003b, 2009; Dahl et al., 2005; Bendle et al., 2006; Yamamoto and Polyak, 2009; Li, 2010; Hoffmann et al., 2013; Boom et al., 2014; Duan et al., 2016). In the Bering Sea, composition of the *n*-alkanes in modern sediments suggests that their distribution patterns can be affected by sedimentation processes related to environment and climate change (Lu et al., 2004). Centennial-scale records of *n*-alkanes and some other biomarkers suggest they might originate mainly from terrestrial and from marine siliceous organisms (Zhang et al., 2007).

In this study, we report terrestrial biomarker records from sediment Core B2-9 recovered from the northern Bering Sea Slope. We focus on the paleoenvironmental implications for variations in the *n*-alkanes and their controlling factors over the past 9.6 ka. The results provide new information about Holocene paleoenvironmental conditions of the Bering Sea and the source regions of its terrestrial vegetation.

2 Oceanographic setting

The principal surface circulation in the Bering Sea Basin is the cyclonic circulating Bering Sea Gyre (BSG), consisting of the East Kamchatka Current (EKC) to the west and the Bering Slope Current (BSC) to the east (Stabeno et al., 1999) (Fig. 1). The Alaskan Stream (AS) imports North Pacific waters via the water routes

Foundation item: The National Natural Science Foundation of China under contract Nos 41030859, 41506223, CHINARE2017-03-02 and IC201105; the Geological Investigation Project of China Geological Survey under contract Nos 12120113006200 and 1212011120044.

*Corresponding author, E-mail: rjwang@tongji.edu.cn

along the Aleutian Arc into the Bering Sea, and drives the BSG (Stabeno et al., 1999; Reed and Stabeno, 1999).

Rivers surrounding the Bering Sea not only import fresh water, but also transport large amounts of terrestrial materials to the shelf and deep basin. Modern observations reveal that the fresh water discharge from Alaskan and Siberian rivers is at least 10 000 m^3/s (Roden, 1967). The Yukon River, the largest river discharging into the Bering Sea, is fundamental to the Bering Sea ecosystem, especially on the northern Bering Sea Shelf, providing most of the freshwater runoff, sediments and dissolved solutes (Roden, 1967; Brabets et al., 2000; Nagashima et al., 2012). The second major contributor is the Anadyr River from eastern Siberia, and the third is the Kuskokwim River from southern Alaska (Roden, 1967; Hood, 1983). Sediments on the Bering Sea Shelf are composed mainly of detrital materials derived from the Alaskan mainland and eastern Siberia, carried by the Yukon/Kuskokwim Rivers and the Anadyr River, respectively (Nagashima et al., 2012). Some small rivers also inject into the Bering Sea, such as the Kamchatka River (Roden, 1967) and the Kvichak and Nushagak Rivers (Sancetta et al., 1984).

3 Materials and methods

3.1 *Sediment core*

Gravity Core B2-9 was recovered from the northern Bering Sea Slope (59°17′32″N, 178°41′50″W, water depth 2 200 m, Fig. 1) during the 1st Chinese National Arctic Expedition in 1999. The sediment core is 231 cm in length and is primarily composed of dark gray diatom mud. The core was sampled at 2-cm intervals and 115 samples in total were obtained.

3.2 *Methods*

All samples were extracted and measured for qualitative and quantitative analysis of organic matter. For this study we mainly analyzed the *n*-alkanes. The freeze-dried samples were ground manually. After adding internal standards of *n*-$C_{24}D_{50}$ and *n*-$C_{19}H_{39}OH$, each sample (2–4 g) was extracted ultrasonically 4–5 times with di-chloromethane/methanol (3:1, v/v). The supernatants were concentrated and then saponified with 6% KOH/methanol at room temperature overnight (approximately 12 h). Neutral components were extracted with *n*-hexane and then were further separated into two sub-fractions by silica gel column chromatography. Hydrocarbons were eluted with *n*-hexane and analyzed directly using a gas chromatograph (GC) under the following GC conditions: an HP-1 capillary column (60 m×0.32 mm×0.17 μm), the injector and flame ionization detector (FID) both at 280°C, splitless injection and helium as the carrier gas with a flow rate of 1.0 mL/min (He et al., 2008). Quantification of biomarkers was performed by integration of the relevant peak areas of the biomarkers of interest and compared with those of the internal standards. Test results using internal standards showed that the recovery ratio of this method was up to 85%, and the standard deviation of four parallel experiments was less than 1%. All analyses were performed at the State Key Laboratory of Marine Geology in Tongji University, Shanghai.

3.3 *Age model*

The age model for Core B2-9 was established by ten Acceler-

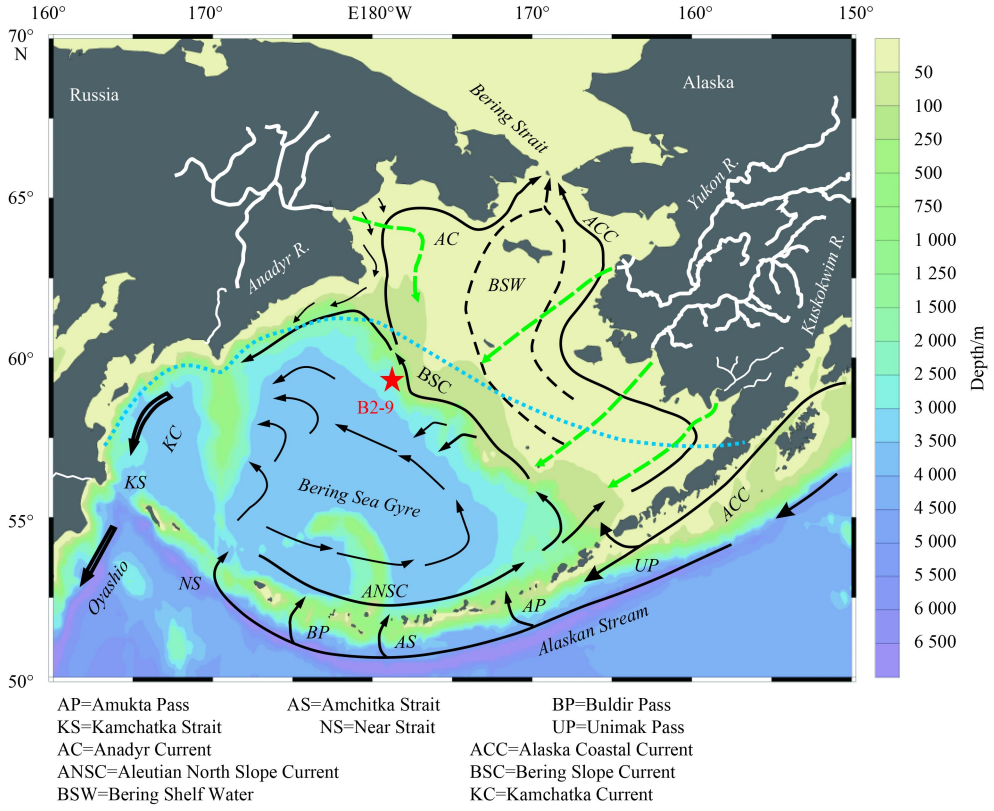

Fig. 1. Modern ocean environment of the Bering Sea and location of Core B2-9. Modern surface circulation systems are shown by black arrows (modified from Stabeno et al., 1999; Grebmeier et al., 2006). The rivers are shown by white lines (redrawn after Sancetta et al., 1984; Brabets et al., 2000; Nagashima et al., 2012). Dashed green arrows show the direction of delivery of materials from rivers, and the dashed blue line indicates the southern edge of the sea ice during 1973–1986 (redrawn after Nagashima et al., 2012).

ator Mass Spectrometry (AMS) ^{14}C dating data, obtained from the organic carbon in sediments and calibrated by Calib 6.0 using a mixed Marine & Northern Hemisphere Atmosphere mixing curve with 75% marine organic carbon (Fairbanks et al., 2005). Linear interpolation was applied between each AMS ^{14}C age (Fig. 2). The core recovered a sediment sequence from 0.98 ka to 9.59 ka with an average sample resolution of 75 years. All ages are reported as calibrated calendar ages. Based on this age model, we calculated

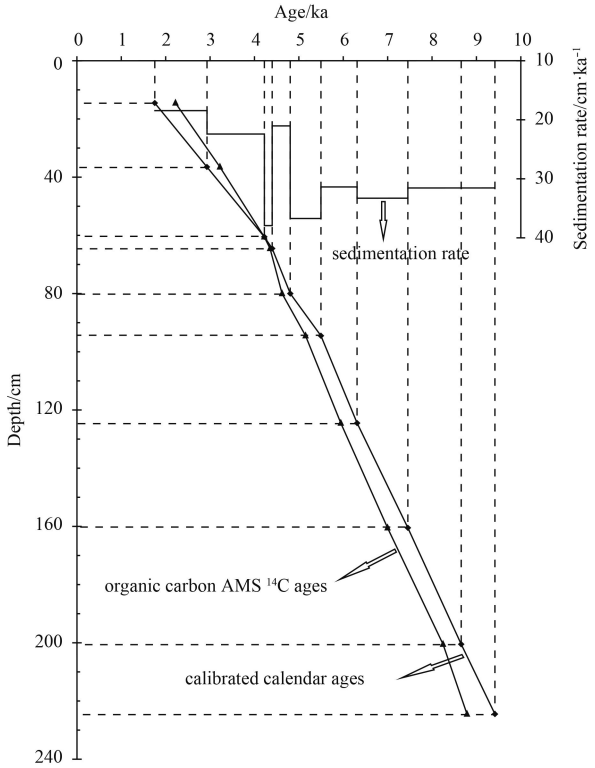

Fig. 2. Age model and sedimentation rate for Core B2-9 from the northern Bering Sea Slope.

the sedimentation rate of Core B2-9, which had gone through three stages overall (Fig. 2).

4 Results and discussion

In general, the *n*-alkanes from terrestrial higher plant waxes range from nC_{21} to nC_{35}, with a clear odd-carbon number dominance, and maximize at nC_{27}, nC_{29}, nC_{31} or nC_{33} (Eglinton and Hamilton, 1967; Meyers, 2003; Hu et al., 2003c). In contrast, the *n*-alkanes produced by marine algae range from nC_{11} to nC_{25}, with nC_{17} or nC_{19} as the most abundant, and without odd-even carbon dominance (Meyers and Ishiwatari, 1993; Hu et al., 2003c; He et al., 2008). Some particular submerged and floating macrophytes, such as *Najas marina*, *Potamogeton* spp., *Vallisneria gigantea*, *Elodea nuttallii* and *Posidonia oceanica*, indicate that the *n*-alkane distributions of these non-emergent vascular plants commonly maximize at nC_{21}, nC_{23} or nC_{25} (Ficken et al., 2000; Meyers, 2003; and references therein), which is significantly different from terrestrial plants. In this paper, we focus on the long-chain *n*-alkane variations, especially the high carbon number *n*-alkanes between nC_{23} and nC_{33}.

4.1 *n-Alkane composition and significance*

In Core B2-9, the *n*-alkanes range from nC_{21} to nC_{35}, with obvious odd-carbon dominance (Fig. 3), similar to previous studies in other oceans. In the following sections we present two features that differ from other studies.

First, nC_{27}, rather than nC_{29} or nC_{31}, shows the highest content among the *n*-alkanes in Core B2-9, consistent with the studies reported by Lu et al. (2004) and Zhang et al. (2007) in the Bering Sea. The nC_{27} content ranges from 90.5 ng/g (Fig. 3a) to 1 187.3 ng/g (Fig. 3b), with an average value of 494.2 ng/g (Fig. 3c). A clear stage characteristic (Fig. 4a) is apparent in the variations. The total odd-carbon number *n*-alkane contents between nC_{25} and nC_{33} (referred to as $\sum_{odd}(nC_{25}\text{–}nC_{33})$) (Fig. 4b) show good correlation (R^2=0.99) to those between nC_{23} and nC_{31} (referred to as $\sum_{odd}(nC_{23}\text{–}nC_{31})$) (Fig. 4c). nC_{27} was the uniquely greatest contributor to the total *n*–alkane content during the Holocene. As shown in Fig. 4d, we take $nC_{27}/\sum_{odd}(nC_{25}\text{–}nC_{33})$ to indicate the contribution ratio of nC_{27} to total *n*-alkane content (referred to as nC_{27} contribution), which ranges from 26% to 44%, and reaches to 32% on average. The high nC_{27} content also leads to almost the same pattern between the total *n*-alkane content and nC_{27}, and the correlation coefficient is 0.98 (R^2). In regions where grasses dominated, nC_{31} is the major *n*-alkane, whereas nC_{27} and nC_{29} are more abundant in sediments where trees dominated (Cranwell, 1973). Ternary plots of the relative proportions of nC_{27}, nC_{29} and nC_{31} in sediments can be used to reconstruct contributions of grasses, shrubs, coniferous trees and deciduous trees surrounding the area studied (Meyers, 2003; and references therein). Our data suggest that abundant woody plants were distributed in the source region during the Holocene, and that the ratio of woody/herbaceous plants was relatively stable.

Second, several instances of rapid decrease in nC_{27} may be attributed to climate deterioration in the source region. Alaskan pollen records show a climatic optimum in the early Holocene of 8–10 ka BP, when communities of *Populus* spp. were more widely distributed than at present. After a transgression in the early Holocene, the forest in eastern Alaska spread to the modern location, and modern vegetation associations had probably developed by that time with the arrival of *Pinus pumila* at 9 ka BP (Lozhkin et al., 1993; Liu et al., 2004). Hence, the rapid decline in

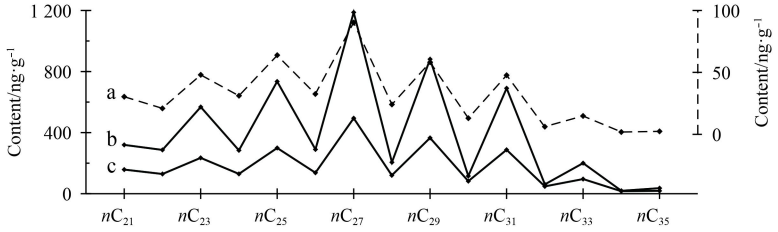

Fig. 3. *n*-alkane distributions and contents in Core B2-9 from the northern Bering Sea Slope. Dashed line a and line b represent the results in the sample with minimum and maximum value of nC_{27} content, respectively. Line c shows the average *n*-alkane content of all samples.

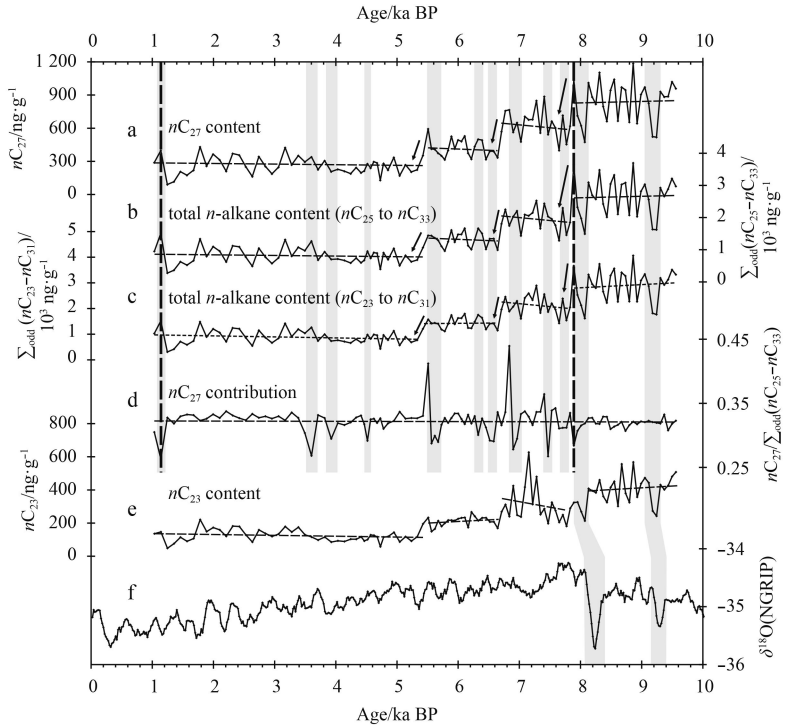

Fig. 4. Variations in total *n*-alkane content and main *n*-alkane compositions for Core B2-9 from the northern Bering Sea Slope during the Holocene. a and e. The variation in nC_{27} and nC_{23}, respectively; b. the trend of the $\Sigma_{odd}(nC_{25}$–$nC_{33})$, and used as the proxy of terrestrial input; c. the trend of the $\Sigma_{odd}(nC_{23}$–$nC_{31})$; d. the contribution rate of $nC_{27}$to the total *n*-alkane content; f. 7-point smoothed δ^{18}O of the ice core from the North Greenland Ice Core Project (NGRIP) during the Holocene (data from Vinther et al., 2006). Solid arrows and horizontal lines show the trends of changes; vertical dashed lines and short gray rectangles indicate the simultaneous variations in different indexes; and long gray rectangles indicate their responses to the rapid climate change during the early Holocene.

nC_{27} between ca. 8–7.8 ka BP may be related to the climatic optimum during the early Holocene. Around ca. 8 ka BP, *Picea glauca* arrived in the northern Alaska Range, and formed a forest tundra association until ca. 6 ka BP. Shrub thickets of *Alnus* spp. established in the region at ca. 6.5 ka BP and *Betula papyrifera* arrived at ca. 6 ka BP. Closed *P. glauca* forests developed at ca. 6 ka BP. *P. mariana* subsequently became important and replaced *P. glauca* as the dominant tree species in the region at ca. 4 ka BP. The establishment of *P. mariana* forests probably reflects the complex response of forest ecosystems to the onset of cooler and moister conditions during the late Holocene (Hu et al., 1996). As the most abundant *n*-alkane from woody plants, nC_{27} productivity would inevitably be affected by changes in vegetation structure. Sedimentary nC_{27} content (Fig. 4a) recorded the progress of rapid cooling at 9.3 ka BP and 8.2 ka BP (Fig. 4f), but the nC_{27} contribution to the total *n*-alkane content (Fig. 4d), which showed the different changes during these two rapid cooling intervals (Fig. 4f), was nearly unchanged, especially around ca. 9.3 ka BP. Further explanations of the reasons for these changes in paleoenvironmental and paleoecological reconstructions need more support from multiple proxies, such as pollen records (e.g., Meyers, 2003). The likely cause will be discussed in Section 4.3 and should be considered in conjunction with changes in the molecular indexes (such as ACL and AI).

nC_{23} in Core B2-9 is maintained at a higher level than nC_{33} in almost all samples. Its contents range from 57.3 ng/g to 627.3 ng/g, with an average of 234.8 ng/g, much more than nC_{33} (95.6 ng/g). The nC_{23} content clearly shows a stepwise decrease from the early to the late Holocene (Fig. 4e), which is similar to nC_{27}, $\Sigma_{odd}(nC_{25}$–$nC_{33})$ and $\Sigma_{odd}(nC_{23}$–$nC_{31})$ during the Holocene (Figs 4a–c), with correlation coefficients (R^2) of 0.85, 0.83 and 0.88, respectively. Such similar fluctuation patterns suggest that nC_{23} may be controlled by some factors that also control nC_{27}. However, previous studies have shown that the high abundance of nC_{23} is mainly produced by some submerged and floating macrophytes (Meyers, 2003; and references therein). For example, the sea-grass known as eelgrass (*Zostera marina* L.) is widespread in coastal and estuarine waters, and its life cycle is controlled by sea water salinity and temperature (Ye and Zhao, 2002; Nejrup and Pedersen, 2008). To exclude the influence of some uncertain factors and maintain uniformity in calculation between the total *n*-alkane content and *n*-alkane indexes (such as carbon preference index (CPI) in the following sections), we remain consistent in this paper in choosing $\Sigma_{odd}(nC_{25}$–$nC_{33})$ as the total *n*-alkane content, used as the proxy for terrestrial inputs (Fig. 4b).

To some extent the changes in nC_{23} indicate changes in the regional climate. According to pollen records from lake sediments in southwestern Alaska, the vegetation structure was similar between southwestern Alaska and north-central Alaska (Hu et al., 1996), and summer temperature during the early Holocene was warmer than at present (Ritchie et al., 1983; Barnosky et al., 1987; Anderson and Brubaker, 1994). As a result, low lake levels and high productivity might have been caused by warm and dry summers (Hu et al., 1996), leading to high nC_{23} productivity over the same period (Fig. 4e). Similar to the nC_{27} (Fig. 4a), nC_{23} content also dropped at ca. 9.3 ka BP and 8.1 ka BP (Fig. 4e), the response of submerged/floating plants to two sudden cold events

recorded by $\delta^{18}O$ in the NGRIP ice core from Greenland (Fig. 4f). nC_{23} content rebounded to a high level at around 7.2 ka BP, different from nC_{27} (Fig. 4a) and the total *n*-alkane content (Fig. 4b). Productivity records from the Arolik Lake, southwestern Alaska, clearly show drops during the two cold periods at around 9.3 ka BP and 8.1 ka BP (Hu et al., 2003a). The cooling would also have suppressed the output of nC_{23} from marine submerged/floating plants. In contrast, the rise in nC_{23} content at ca. 7.2 ka BP might have been caused by increasing productivity in lakes, and may also reflect the distinction between nC_{23} and terrestrial *n*-alkanes as the proxies of climate change (e.g., Ficken et al., 2000).

4.2 *Terrestrial input changes and controlling factors*

The total *n*-alkane content ranged from 275.3 ng/g to 3 694.8 ng/g and 1 681.2 ng/g on average during the past 9.6 ka BP, with an overall decreasing trend from the early to the late Holocene. This kind of decline change has four clearly periodic stages (Fig. 4b). During Stage I, ca. 9.6–7.8 ka BP, total *n*-alkane content underwent a rapid fluctuation with high amplitude, and its average value was up to 2 657.3 ng/g. In Stage II, ca. 7.8–6.7 ka BP, both the frequency and amplitude of changes in the total *n*-alkane content were reduced, showing a slightly upward trend, but lower than Stage I, with an average of 1 948.7 ng/g. In Stage III, ca. 6.7–5.4 ka BP, the total *n*-alkane content decreased further, with an average of 1 304.6 ng/g. Its trend was similar to Stage II, but more stable. The total *n*-alkane content was relatively steady in Stage IV, from ca. 5.4 BP, with the minimum average value (814.2 ng/g) of the four stages, but during the Holocene this was still significantly higher than in other seas, such as the Southern Ocean (Li and Wang, 2004) and the northern South China Sea (He et al., 2008).

In general, the deposit of *n*-alkanes in marine sediments is controlled by two factors: the *n*-alkane productivity of land plants and the environmental conditions of transportation. We argue that, in the study area, the most important factor of terrestrial input changes during the Holocene was sea-level change. Global sea levels rose from about –50 m (compared with the modern level) at ca. 11 ka and reached the modern level at ca. 6 ka (Huang et al., 2009; and references therein). As a result, the shoreline of Alaska and Siberia would have shifted away from the core location and the wide, exposed northeastern continental shelf of the Bering Sea would have been submerged again, causing a decreased vegetation coverage area. During sea-level rise, the plant residues were transported by currents to the slope area, and further into the basin. The rising sea level also moved estuaries such as that of the Yukon River back inland, which extended the delivery distance of terrestrial materials from the estuary to sedimentary sites in the sea. The rising sea level not only reduced the distribution range of terrestrial vegetation, but also extended the distance between river estuary and sedimentary area on the northern slope. Therefore, the decline in total *n*-alkane input during ca. 9.6–5.4 ka BP (Fig. 4c) was the result of a reduction in terrestrial materials. From ca. 6 ka BP the influence of sea-level change weakened gradually. However, Hopkins (1967) has pointed out that there was a transgression in the Bering Sea between ca. 6 ka BP and 5 ka BP, which was also recorded in sediments of Core B2-9. The total *n*-alkane content dropped by nearly half in 200 years, and this was the last stepwise decrease during the Holocene (Fig. 4c).

Continuous sea-level rise had a gradual impact on the total *n*-alkane content; its decrease around ca. 6.7 ka BP and ca. 7.8 ka BP (Fig. 4c) may not only have been controlled by sea level, but also have been related to the climate and vegetation abundance in the source region. Pollen data from lake sediments in southwestern Alaska indicate that winter precipitation and spring temperature both increased from ca. 9.8 ka BP (Hu et al., 1995). During ca. 11–7 ka BP, the Holocene Thermal Maximum occurred both in central Beringia and western Alaska (Kaufman et al., 2004, and references therein). Katsuki et al. (2009) pointed out that the vast area of southwestern Alaska was, overall, warm and wet at this time because of the impact of the Aleutian Low. Such a climate favored terrestrial vegetation growth and density, which produced more *n*-alkanes. After ca. 7 ka BP the climate of southwestern Alaska changed from warm and wet to cold and wet under the influence of the enhanced Aleutian Low. These changes might not only have caused the shrinkage in the vegetation area, but also altered the strength and direction of the prevailing winds. By then, the *n*-alkanes would have been delivered mainly by river discharge. Finally, the total *n*-alkane content dropped at ca. 6.7 ka BP (Fig. 4c). The controlling factor for the rapid decline at ca. 7.8 ka might be slightly different from that of other declines. A variety of paleoenvironmental records from Alaska and adjacent areas in Canada for the period ca. 11–8 ka BP suggest that this region experienced a period of relatively warm summers, presumably caused by a pronounced maximum in summer insolation in northern high latitudes (Hu et al., 1996, and references therein). Hence, in Stage I, the high *n*-alkanes may be mainly caused by high terrestrial vegetation productivity. Total *n*-alkane content shows a 200-year episode of extremely low values around 8.0 ka BP (Fig. 4c), even lower than the average value of Stage II. This change is probably a response to the "8.2 ka event" as recorded in the Greenland ice core $\delta^{18}O$ (Alley and Ágústsdóttir, 2005), which was a rapid cold event lasting only about 400 years (Fig. 4f). Another clearly minimum value event in ca. 9.3–9.1 ka BP was the marked response to the 9.3 ka cold event (Fig. 4f). The production of terrestrial vegetation was severely reduced during the cold spells, as confirmed by Hu et al. (1996): the vegetation community appeared to have declined in abundance near the end of the early Holocene between ca. 11 ka BP and 8 ka BP. The impact on terrestrial *n*-alkane production was irreversible, especially during the 8.2 ka BP event, and directly induced the shift from Stage I to Stage II.

Seasonal sea ice may have been another factor influencing *n*-alkane input. Seasonal sea ice retreated gradually into the inner continental shelf in the Holocene (Katsuki et al., 2009). During the early Holocene, sea ice retreated significantly in the Bering Sea (Méheust et al., 2016). From the mid-Holocene, sea ice rarely extended to the core site of B2-9 (Katsuki et al., 2009). Thus, although its influence cannot be ignored, sea ice may not be a major controlling factor. Similarly, the influence of sedimentation rate on *n*-alkane contents may also be limited. According to Fig. 2, the sedimentation rate of Core B2-9 shows a change in phase with three stages, which is different from the characteristically stages of the *n*-alkanes (Figs 4a, b). Before ca. 5.4 ka BP, the sedimentation rate was relatively stable at ca. 31.4 cm/ka on average, but the nC_{27} (Fig. 4a) and total *n*-alkane content (Fig. 4b) dropped at ca. 9.6 ka BP, 7.8 ka BP and 5.4 ka BP. In contrast, the *n*-alkanes were relatively stable since ca. 5.4 ka BP, while the sedimentation rate underwent several rapid changes between ca. 5.4 ka BP and 4.2 ka BP, and remained at a lower level since ca. 4.2 ka BP. This distinction may suggest that there is no direct relationship between them.

4.3 *Variations in molecular indexes and their implications*

The molecular indexes of *n*-alkanes based on their compositions, such as CPI, ACL, alkane index (AI) and nC_{31}/nC_{27} ratio,

have been used to estimate the sources of these *n*-alkanes and to reconstruct the vegetation type and climate of the source region. The odd-carbon preference of the *n*-alkanes of terrestrial higher plants decreases with degradation and diagenesis, and the CPI of fresh land vegetation *n*-alkane is generally greater than 3; thus CPI has been used to indicate *n*-alkane source and its degree of maturation (He et al., 2008, and Table 1 therein). ACL, AI and nC_{31}/nC_{27} ratios are established on the basis of the modern observation that the most abundant *n*-alkanes have different carbon numbers in different types of vegetation. As discussed above, both grass and trees produce nC_{27}, nC_{29} and nC_{31}, but usually nC_{31} is most abundant in grass while nC_{27} or nC_{29} is most abundant in trees. Thus, the increasing values of ACL, AI and nC_{31}/nC_{27} ratios indicate a higher contribution from grass (Maffei, 1996; Zhang et al., 2006).

CPI ranges from 1.47 to 5.19 in Core B2-9, with an average of 3.63. Most values are greater than 3, indicating that the *n*-alkanes are primarily derived from terrestrial vegetation, rather than from fossil *n*-alkanes with high maturation. CPI shows a descending trend overall, suggesting that the contribution of terrestrial *n*-alkanes to the total *n*-alkanes gradually reduced. Sea levels reached their modern levels by ca. 6 ka BP, which may be the most important reason for the CPI changes before ca. 5.4 ka BP. Sea-level rise would have reduced the input from terrestrial *n*-alkanes but rarely affected fossil *n*-alkanes. From ca. 5.4 ka BP, the nC_{27} and total *n*-alkane content remained at a steady level (Figs 4a, b); however, CPI continued its downward tendency (Fig. 5a), although its average value was 3.29 during this stage. Hence, the changes in CPI after ca. 5.4 ka BP may have been caused by increased contributions from fossil *n*-alkanes, and not by decreasing *n*-alkanes. At the same time, the variations in ACL and nC_{31}/nC_{27} ratios show nearly the same stable trend. ACL, nC_{31}/nC_{27} ratio and AI did not show any special pattern of variation (Figs 5b–d). Considering the contribution of nC_{27} to total *n*-alkanes, we argue that vegetation structure in source regions maintained a relatively stable state during the Holocene, and

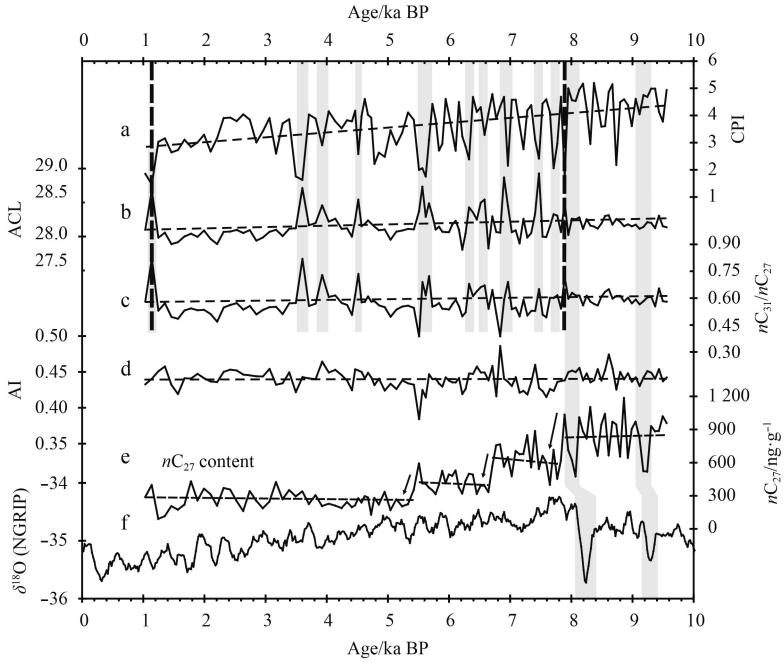

Fig. 5. Variations in *n*-alkane molecular indexes for Core B2-9 on the northern Bering Sea Slope during the Holocene. a–d. The variations in carbon preference index (CPI), average chain length (ACL), ratio of nC_{31}/nC_{27}, and alkane index (AI), respectively; e and f. the variation in nC_{27} and 7-point smoothed $\delta^{18}O$ records (data from Vinther et al., 2006). Solid arrows and horizontal lines show the trends of data; vertical dashed lines and short gray rectangles indicate the synchronization between nC_{27} CPI, ACL and nC_{31}/nC_{27}; and long gray rectangles indicate their response to the rapid climate change during the early Holocene.

woody plants predominated over herbaceous plants in most of intervals.

Variation patterns in these indexes were not uniform during the Holocene. First, several peaks in the ACL and nC_{31}/nC_{27} ratio corresponded to low CPI (Fig. 5a) and low nC_{27} contributions (Fig. 4d) in some short periods, such as ca. 7.9 ka BP and ca. 1.1 ka BP. These peaks reveal that the herbaceous plant contribution increased as the woody plant contribution decreased. Low CPI indicates an increased fossil *n*-alkane contribution, and low nC_{27} contribution indicates the declined woody plant *n*-alkane contribution. However, the nC_{27} production and total *n*-alkane content have similar change patterns. Therefore, the growth rate of woody plant *n*-alkane contribution was lower than that of herbaceous plant *n*-alkane and fossil *n*-alkane, even though woody plants still had high productivity. One possible explanation is that, during these short periods, the climate might have become dry and cold in the source regions, the stronger terrestrial weathering provided considerably more fossil *n*-alkanes and herbaceous plants flourished. There is some evidence for this. According to previous studies the tundra vegetation communities in the Arctic often comprised mosses, lichens, erect shrubs, graminoids and prostrate shrubs, and the vegetation community on the land north of the Bering Sea was mainly tundra (Walker et al., 2005; Bratsch et al., 2016). The Yukon watershed in Alaska may be taken as an example. The Yukon River is the main terrestrial input source of the Bering Sea: approximately 20% of the catchment is covered by spruce forest such as *Picea glauca* and black *P. mariana* (Brabets et al., 2000), about 40% by grassland, 20% by

shrubland and 8% by open water and wetlands associated with the lowland areas (Amon et al., 2012; and references therein). However, further research will be needed to provide more evidence for this explanation.

Second, similar to the nC_{27} contribution (Fig. 4d), these *n*-alkane indexes did not show any significant changes during the "8.2 ka event" and "9.3 ka event" intervals (Figs 5a–d). The most likely reason for such discrepancies was the effect of drastic cooling over a short time. According to Alley and Ágústsdóttir (2005), the cooling event at ca. 8.2 ka BP might have caused the low water level and a declined spruce in Alaska (Andreev and Peteet, 1997; Mason et al., 2001), indicating a decrease in aquatic productivity and woody plant production. Mason et al. (2001) further suggested that extensive weathering and erosion in these regions, which supported an increase in fossil *n*-alkane production at that time. However, glacial advance in the St. Elias Mountains culminated at about the same time (Denton and Karlén, 1973), which might indicate that the transportation of fossil *n*-alkanes was restricted to some extent. Moreover, Brubaker et al. (2001) indicated that the herb pollen percentage decreased more than the percentage of xylophyta in sediments from six lakes in southwestern Alaska at ca. 9.3 ka BP. As a result of these changes, although the production of alkanes was limited during these two rapid cooling periods, the contribution of nC_{27} (Fig. 4d), CPI, ACL, nC_{31}/nC_{27} ratio and AI showed no significant decrease or increase. Climate signal transmission between sea and land, and early diagenesis of sediments, may also have caused these differences.

5 Conclusions

In this study, based on extraction and measurement of high-resolution terrestrial biomarkers in Core B2-9 sediments from the northern Bering Sea Slope, we present variations in *n*-alkanes, terrestrial input and vegetation records over the last 9.6 ka. The results are summarized as follows:

(1) Long-chain *n*-alkane distribution has two special features: (a) nC_{27} is the main carbon peak in virtually every sample, and has the greatest contribution rate to the total *n*-alkane content, which might be related to the abundant woody plants and their spatial distribution in the source region; and (b) nC_{23} is another *n*-alkane with a relatively high content, with variations similar to those of nC_{27}, mainly derived from submerged plants which were widely distributed along coastal areas of the northern hemisphere.

(2) The total *n*-alkane record indicates four relatively stable stages, and dropped quickly at ca. 7.8 ka BP, ca. 6.7 ka BP and ca. 5.4 ka BP, mostly controlled by sea-level rise, climate changes and vegetation distribution in the source region, respectively.

(3) The gradually decreased trend and high value of CPI (>3) in the Holocene indicate that the *n*-alkanes primarily originated from land plants. The ACL and nC_{31}/nC_{27} ratio show nearly the same stable state during the whole Holocene, suggesting relatively steady woody/herbaceous plants and dominant woody plants in most intervals.

(4) In several short periods, low nC_{27} contribution and CPI corresponding to high ACL and nC_{31}/nC_{27} ratio, with the contemporary changes in total *n*-alkane and nC_{27} content, reveal that the growth rate of woody plant *n*-alkane contribution was lower than that of herbaceous plants and fossil *n*-alkanes under the particular climate conditions of the source region.

Acknowledgements

The research was a part of "First China Arctic Expedition" (referred to as CHINARE-1999), which organized by Chinese Arctic and Antarctic Administration of State Oceanic Administration and funded by Ministry of Finance of PR China. The authors thank all the cruise members of CHINARE-1999 for collecting samples. Li Wenbao (Tongji University) and Lu Bing (SIO) are acknowledged for their analytical support and suggestions on the manuscript.

References

Alley R B, Ágústsdóttir A M. 2005. The 8k event: cause and consequences of a major Holocene abrupt climate change. Quaternary Science Reviews, 24(10–11): 1123–1149

Amon R M W, Rinehart A J, Duan S, et al. 2012. Dissolved organic matter sources in large Arctic rivers. Geochimica et Cosmochimica Acta, 94: 217–237

Anderson P M, Brubaker L B. 1994. Vegetation history of northcentral Alaska: a mapped summary of late-Quaternary pollen data. Quaternary Science Reviews, 13(1): 71–92

Andreev A A, Peteet D M. 1997. An 8100 year record of vegetation changes from a Peat site near Fairbanks, Alaska. Florissant, CO: Beringian Paleoenvironments Workshop, 16–18

Barnosky C W, Anderson P M, Bartlein P J. 1987. The northwestern U.S. during deglaciation: vegetational history and paleoclimatic implications. In: Ruddiman W F, Wright Jr H E, eds. North America and Adjacent Oceans during the Last Deglaciation. Boulder, Colorado: Geological Society of America, 289–321

Bendle J A, Kawamura K, Yamazaki K. 2006. Seasonal changes in stable carbon isotopic composition of *n*-alkanes in the marine aerosols from the western North Pacific: implications for the source and atmospheric transport. Geochimica et Cosmochimica Acta, 70(1): 13–26

Boom A, Carr A S, Chase B M, et al. 2014. Leaf wax *n*-alkanes and $\delta^{13}C$ values of CAM plants from arid southwest Africa. Organic Geochemistry, 67: 99–102

Brabets T P, Wang B, Meade R H. 2000. Environmental and hydrologic overview of the Yukon River Basin, Alaska and Canada. Water-Resources Investigations Report 99-4204. Anchorage, Alaska: US Geological Survey

Bratsch S N, Epstein H E, Buchhorn M, et al. 2016. Differentiating among four arctic tundra plant communities at Ivotuk, Alaska using field spectroscopy. Remote Sensing, 8(1): 51

Brubaker L B, Anderson P M, Hu Fengsheng. 2001. Vegetation ecotone dynamics in Southwest Alaska during the Late Quaternary. Quaternary Science Reviews, 20(1–3): 175–188

Cranwell P A. 1973. Chain-length distribution of *n*-alkanes from lake sediments in relation to post-glacial environmental change. Freshwater Biology, 3(3): 259–265

Dahl K A, Oppo D W, Eglinton T I, et al. 2005. Terrigenous plant wax inputs to the Arabian Sea: implications for the reconstruction of winds associated with the Indian Monsoon. Geochimica et Cosmochimica Acta, 69(10): 2547–2558

Denton G H, Karlén W. 1973. Holocene climatic variations—their pattern and possible cause. Quaternary Research, 3(2): 155–174

Duan Yi, Zhao Yang, Wu Yingzhong, et al. 2016. δD values of *n*-alkanes in sediments from Gahai Lake, Gannan, China: implications for sources of organic matter. Journal of Paleolimnology, 56(2–3): 95–107

Eglinton G, Hamilton R J. 1967. Leaf epicuticular waxes. Science, 156(3780): 1322–1335

Fairbanks R G, Mortlock R A, Chiu T C, et al. 2005. Radiocarbon calibration curve spanning 0 to 50,000 years BP based on paired $^{230}Th/^{234}U/^{238}U$ and ^{14}C dates on pristine corals. Quaternary Science Reviews, 24(16–17): 1781–1796

Ficken K J, Li B, Swain D L, et al. 2000. An *n*-alkane proxy for the sedimentary input of submerged/floating freshwater aquatic macrophytes. Organic Geochemistry, 31(7–8): 745–749

Gorbarenko S A, Wang P, Wang R, et al. 2010. Orbital and suborbital environmental changes in the southern Bering Sea during the last 50 kyr. Palaeogeography, Palaeoclimatology, Palaeoecology, 286(1–2): 97–106

Grebmeier J M, Cooper L W, Feder H M, et al. 2006. Ecosystem dynamics of the Pacific-influenced northern Bering and Chukchi Seas in the Amerasian Arctic. Progress in Oceanography, 71(2–4): 331–361

He Juan, Zhao Meixun, Li Li, et al. 2008. Sea surface temperature and terrestrial biomarker records of the last 260 ka of core MD05-2904 from the northern South China Sea. Chinese Science Bulletin, 53(15): 2376–2384

Hoffmann B, Kahmen A, Cernusak L A, et al. 2013. Abundance and distribution of leaf wax *n*-alkanes in leaves of Acacia and Eucalyptus trees along a strong humidity gradient in northern Australia. Organic Geochemistry, 62: 62–67

Hood D W. 1983. The Bering Sea. In: Ketchum B H, ed. Estuaries and Enclosed Seas. New York: Elsevier, 337–373

Hopkins D M. 1967. Quaternary marine transgressions in Alaska. In: Hopkins D M, ed. The Bering Land Bridge. Stanford: Stanford University Press, 47–90

Hu Fengsheng, Brubaker L B, Anderson P M. 1996. Boreal ecosystem development in the northwestern Alaska range since 11,000 yr B.P. Quaternary Research, 45(2): 188–201

Hu Fengsheng, Kaufman D, Yoneji S, et al. 2003a. Cyclic variation and solar forcing of Holocene climate in the Alaskan subarctic. Science, 301(5641): 1890–1893

Hu Jianfang, Peng Ping'an, Chivas A R. 2009. Molecular biomarker evidence of origins and transport of organic matter in sediments of the Pearl River estuary and adjacent South China Sea. Applied Geochemistry, 24(9): 1666–1676

Hu Jianfang, Peng Ping'an, Fang Dianyong, et al. 2003b. No aridity in Sunda Land during the Last Glaciation: evidence from molecular-isotopic stratigraphy of long-chain *n*-alkanes. Palaeogeography, Palaeoclimatology, Palaeoecology, 201(3–4): 269–281

Hu Jianfang, Peng Ping'an, Jia Guodong, et al. 2002. Biological markers and their carbon isotopes as an approach to the paleoenvironmental reconstruction of Nansha area, South China Sea, during the last 30 ka. Organic Geochemistry, 33(10): 1197–1204

Hu Jianfang, Peng Ping'an, Jia Guodong, et al. 2003c. A biomarker and isotopic approach for the paleoenvironmental reconstruction, Nansha area, South China Sea since the last 30 ka. Acta Sedimentologica Sinica (in Chinese), 21(2): 211–218

Huang Xiaohui, Wang Rujian, Jian Zhimin. 2009. Holocene terrigenous input changes in the northern Okinawa Trough and their paleoclimatic implications. Marine Geology & Quaternary Geology (in Chinese), 29(5): 73–82

Hwang J, Kim M, Park J, et al. 2014. Alkenones as tracers of surface ocean temperature and biological pump processes on the Northwest Atlantic margin. Deep Sea Research Part I: Oceanographic Research Papers, 83: 115–123

Katsuki K, Khim B K, Itaki T, et al. 2009. Land-sea linkage of Holocene paleoclimate on the Southern Bering Continental Shelf. The Holocene, 19(5): 747–756

Kaufman D S, Ager T A, Anderson N J, et al. 2004. Holocene thermal maximum in the western Arctic (0–180°W). Quaternary Science Reviews, 23(5–6): 529–560

Li Li, Wang Pinxian. 2004. Marine "bio-pumps": biomarkers of marine phytoplankton. Marine Geology & Quaternary Geology (in Chinese), 24(4): 73–79

Li Wenbao. 2010. The paleoceangraphic records during the last 2 Ma in Southern Tasman Sea of Southern Ocean and comparison between high latitude and low latitude oceans [dissertation]. Shanghai: Tongji University

Liu Yanguang, Shi Xuefa, Lü Hailong. 2004. Advances in paleoceanographic studies on the Japan Sea, Okhotsk Sea and Bering Sea. Advances in Marine Science (in Chinese), 22(4): 519–530

Lozhkin A V, Anderson P M, Eisner W P, et al. 1993. Late quaternary lacustrine pollen records from southwestern Beringia. Quaternary Research, 39(3): 314–324

Lu Bing, Chen Ronghua, Zhou Huaiyang, et al. 2005. Oceanic environmental changes of subarctic Bering Sea in recent 100 years: evidence from molecular fossils. Science in China Series D: Earth Sciences, 48(4): 555–564

Lu Bing, Zhou Huaiyang, Chen Ronghua, et al. 2004. The composition characteristics of *n*-alkanes in the modern sediments of the Arctic and the comparison with that of sea areas of different latitudes. Chinese Journal of Polar Research (in Chinese), 16(4): 281–294

Maffei M. 1996. Chemotaxonomic significance of leaf wax alkanes in the Gramineae. Biochemical Systematics and Ecology, 24(1): 53–64

Martínez-Garcia A, Rosell-Melé A, Geibert W, et al. 2009. Links between iron supply, marine productivity, sea surface temperature, and CO_2 over the last 1.1 Ma. Paleoceanography, 24(1): PA1207

Mason O K, Bowers P M, Hopkins D M. 2001. The early Holocene Milankovitch thermal maximum and humans: adverse conditions for the Denali complex of eastern Beringia. Quaternary Science Reviews, 20(1–3): 525–548

Mead R, Xu Yunping, Chong J, et al. 2005. Sediment and soil organic matter source assessment as revealed by the molecular distribution and carbon isotopic composition of *n*-alkanes. Organic Geochemistry, 36(3): 363–370

Méheust M, Stein R, Fahl K, et al. 2016. High-resolution IP_{25}-based reconstruction of sea-ice variability in the western North Pacific and Bering Sea during the past 18,000 years. Geo-Marine Letters, 36(2): 101–111

Meyers P A, Ishiwatari R. 1993. Lacustrine organic geochemistry—an overview of indicators of organic matter sources and diagenesis in lake sediments. Organic Geochemistry, 20(7): 867–900

Meyers P A. 1997. Organic geochemical proxies of paleoceanographic, paleolimnologic, and paleoclimatic processes. Organic Geochemistry, 27(5–6): 213–250

Meyers P A. 2003. Applications of organic geochemistry to paleolimnological reconstructions: a summary of examples from the Laurentian Great Lakes. Organic Geochemistry, 34(2): 261–289

Nagashima K, Asahara Y, Takeuchi F, et al. 2012. Contribution of detrital materials from the Yukon River to the continental shelf sediments of the Bering Sea based on the electron spin resonance signal intensity and crystallinity of quartz. Deep Sea Research Part II: Topical Studies in Oceanography, 61–64: 145–154

Nejrup L B, Pedersen M F. 2008. Effects of salinity and water temperature on the ecological performance of *Zostera marina*. Aquatic Botany, 88(3): 239–246

Ohkouchi N, Kawamura K, Kawahata H, et al. 1997. Latitudinal distributions of terrestrial biomarkers in the sediments from the Central Pacific. Geochimica et Cosmochimica Acta, 61(9): 1911–1918

Reed R K, Stabeno P J. 1999. The Aleutian north slope current. In: Loughlin T R, Ohtani K, eds. Dynamics of the Bering Sea. Fairbanks: University of Alaska Sea Grant, 177–191

Ritchie J C, Cwynar L C, Spear R W. 1983. Evidence from north-west Canada for an early Holocene Milankovitch thermal maximum. Nature, 305(5930): 126–128

Roden G I. 1967. On river discharge into the northeastern Pacific Ocean and the Bering Sea. Journal of Geophysical Research, 72(22): 5613–5629

Rosell-Melé A, Prahl F G. 2013. Seasonality of UK'37 temperature estimates as inferred from sediment trap data. Quaternary Science Reviews, 72: 128–136

Sancetta C, Heusser L, Labeyrie L, et al. 1984. Wisconsin—Holocene paleoenvironment of the Bering Sea: evidence from diatoms, pollen, oxygen isotopes and clay minerals. Marine Geology, 62(1–2): 55–68

Stabeno P J, Schumacher J D, Ohtani K. 1999. The physical oceanography of the Bering Sea. In: Loughlin T R, Ohtani K, eds. Dynamics of the Bering Sea. Fairbanks: University of Alaska Sea Grant, 1–28

Takahashi K. 1998. The Bering and Okhotsk Seas: modern and past paleoceanographic changes and gateway impact. Journal of Asian Earth Sciences, 16(1): 49–58

Takahashi K. 1999. Paleoceanographic changes and present environment of the Bering Sea. In: Loughlin T R, Ohtani K, eds. Dynamics of the Bering Sea. Fairbanks: University of Alaska Sea Grant, 365–385

Vinther B M, Clausen H B, Johnsen S J, et al. 2006. A synchronized dating of three Greenland ice cores throughout the Holocene. Journal of Geophysical Research, 111(D13): D13102, doi: 10.1029/2005JD006921

Walker D A, Raynolds M K, Daniëls F J A, et al. 2005. The circumpolar Arctic vegetation map. Journal of Vegetation Science, 16(3): 267–282

Wang Rujian, Xiao Wenshen, Li Qianyu, et al. 2006. Polycystine radiolarians in surface sediments from the Bering Sea Green Belt area and their ecological implication for paleoenvironmental reconstructions. Marine Micropaleontology, 59(3–4): 135–152

Xing Lei, Zhao Meixun, Zhang Hailong, et al. 2008. Biomarker reconstruction of phytoplankton productivity and community structure changes in the middle Okinawa Trough during the last 15 ka. Chinese Science Bulletin, 53(16): 2552–2559

Yamamoto M, Polyak L. 2009. Changes in terrestrial organic matter input to the Mendeleev Ridge, western Arctic Ocean, during the Late Quaternary. Global and Planetary Change, 68(1–2): 30–37

Ye Chunjiang, Zhao Kefu. 2002. Advances in the study on the marine higher plant Eelgrass (*Zostera marina* L.) and its adaptation to submerged life in seawater. Chinese Bulletin of Botany (in Chinese), 19(2): 184–193

Zhang Haisheng, Pan Jianming, Chen Jianfang, et al. 2007. Biomarkers in sediments in the Arctic areas and ecological environmental response. Marine Geology & Quaternary Geology (in Chinese), 27(2): 41–49

Zhang Zhaohui, Zhao Meixun, Eglinton G, et al. 2006. Leaf wax lipids as paleovegetational and paleoenvironmental proxies for the Chinese Loess Plateau over the last 170 kyr. Quaternary Science Reviews, 25(5–6): 575–594

Zhao Meixun, Mercer J L, Eglinton G, et al. 2006. Comparative molecular biomarker assessment of phytoplankton paleoproductivity for the last 160 kyr off Cap Blanc, NW Africa. Organic Geochemistry, 37(1): 72–97